

Proceedings of the Fifth Annual LHCP

March 13, 2022

Soft QCD

ŠÁRKA TODOROVA-NOVÁ

*On behalf of the ALICE, ATLAS, CMS, LHCb and TOTEM Collaborations,
LAPP, CNRS/IN2P3 and Université Savoie Mont Blanc, Annecy-le-Vieux, France*

ABSTRACT

The talk contains an overview of recent experimental results obtained by the LHC experiments. The measured inclusive event properties, as well as various correlation phenomena, are compared with predictions of phenomenological models.

PRESENTED AT

The Fifth Annual Conference
on Large Hadron Collider Physics
Shanghai Jiao Tong University, Shanghai, China
May 15-20, 2017

1 Introduction

The understanding of the bulk of the particle production at the LHC has a major impact on the search of new physics phenomena. The measurements of the inclusive cross-section, of the inclusive single particle spectra, and the measurements of various correlation phenomena serve both as a test of the predictions of the phenomenological models and as an input for their improvement.

2 Inclusive cross-section measurements

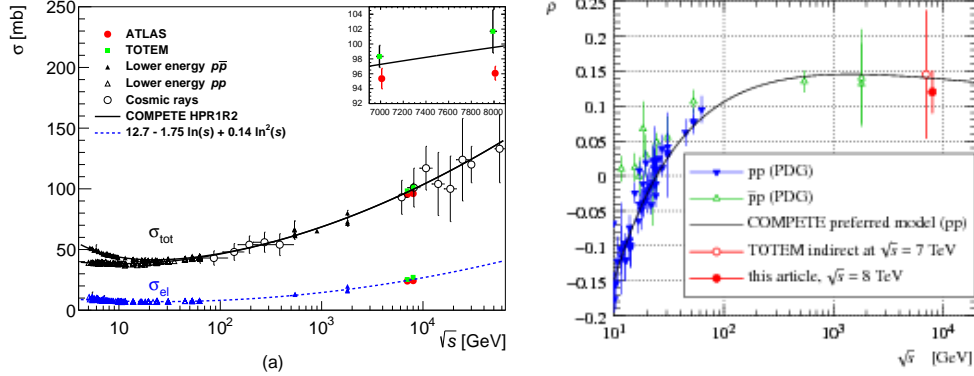


Figure 1: Left: The elastic and the total proton-proton cross sections versus \sqrt{s} [1]. Right: The ρ -parameter versus \sqrt{s} [3] .

Figure 1(left) shows the compilation of the measurements of the elastic and the total proton-proton cross section as a function of the center-of-mass energy, including the ATLAS and TOTEM measurements at $\sqrt{s}=7\text{TeV}$ and 8TeV , compared to the global fit (plot taken from [1]). The total cross section is obtained from the measured elastic scattering via the optical theorem $\sigma_{tot}^2 = 16\pi(\hbar c)^2/(1 + \rho^2)d\sigma_{el}/dt|_{t \rightarrow 0}$. The TOTEM measurement at $\sqrt{s}=8\text{TeV}$ uses a luminosity-independent method [2]. Figure 1(right) shows the energy dependence of the ρ parameter including the TOTEM measurement in the region of very low momentum transfer t sensitive to the Coulomb-nuclear interference [3].

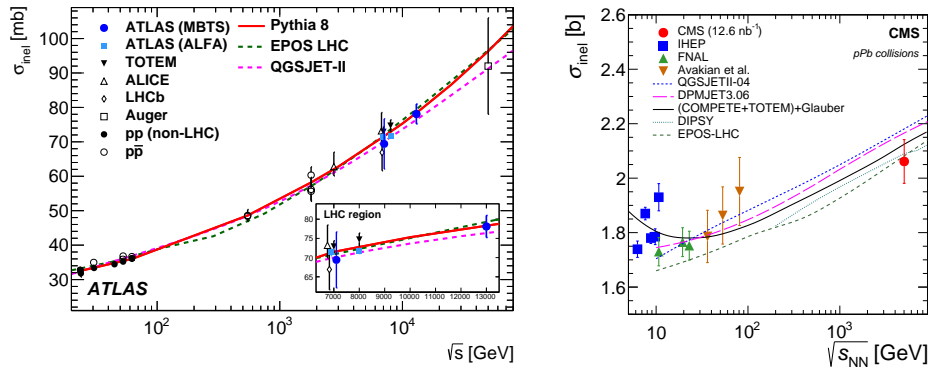


Figure 2: Left: The inelastic proton-proton cross section versus \sqrt{s} . The LHC data points are slightly shifted horizontally for better visibility [4]. Right: The inelastic proton-Pb cross section versus \sqrt{s} [5].

Figure 2 shows the compilations of the measurements of the inelastic proton-proton and proton-Pb cross sections as a function of the center-of-mass energy, up to $\sqrt{s} = 13\text{ TeV}$, compared to the predictions of several MC generators. A good agreement is observed between measurements and the model expectations.

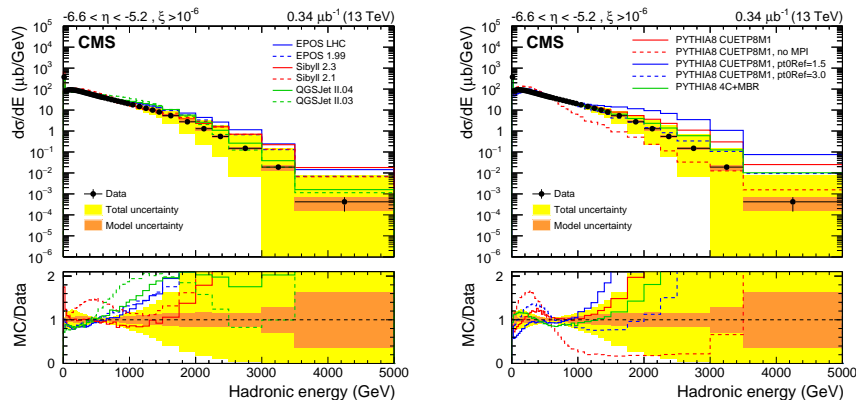


Figure 3: Differential cross section as a function of the hadronic energy in the region $-6.6 < \eta < -5.2$ for events with $\xi > 10^{-6}$. The left panel shows the data compared to MC event generators mostly developed for cosmic ray induced air showers, and the right panel to different PYTHIA 8 tunes [6].

The electromagnetic, hadronic, and total energy spectra of particles produced at very forward pseudo-rapidities ($-6.6 < \eta < -5.2$) have been measured with the CASTOR calorimeter of the CMS experiment in proton-proton collisions at a $\sqrt{s} = 13$ TeV. The experimental distributions, fully corrected for detector effects, are compared to the predictions of various Monte Carlo event generators commonly used in high energy cosmic ray physics (EPOS, QGSJetII, and Sibyll), and those of different tunes of PYTHIA 8 (Figure 3). None of the generators considered describe all features seen in the data. The present measurements are particularly sensitive to the modeling of multiparton interactions (MPI) that dominate particle production in the underlying event at forward rapidities in pp collisions. Event generators developed for modeling high energy cosmic ray air showers, tuned to LHC measurements at 0.9, 7, and 8 TeV, agree better with the present data than those tuned to Tevatron results alone. This is especially true for QGSJetII and Sibyll. However, all these models underestimate the muon production rate in extensive air showers because of their inaccurate description of the hadronic shower component [6].

3 Inclusive charged particle spectra in pp collisions

Figure 4 shows the comparison of the inclusive charged-particle spectra measured by ATLAS [7] at $\sqrt{s} = 13$ TeV with the predictions of PYTHIA8 (A2 and Monash tune), EPOS LHC and QGSJET II-04 event generators. Overall, the data are best described by EPOS. The QSGJET-II generator, which has no model for colour coherence effects, describes the p_T dependence poorly.

3.1 Underlying event spectra in pp collisions

Charged-particle distributions sensitive to the underlying event have been measured by the ATLAS detector in low-luminosity proton-proton collisions at $\sqrt{s} = 13$ TeV [8]. The angular distribution of energy and particle flows with respect to the charged particle with highest transverse momentum (the leading particle) is defined as shown in Figure 5 (left). Figure 5 shows the measurement of the average charged-particle density for the $p_T^{\text{lead}} > 1$ GeV and $p_T^{\text{lead}} > 10$ GeV. The results are compared to the predictions of various Monte Carlo event generators, experimentally establishing the level of underlying-event activity at LHC Run 2 energies and providing inputs for the development of event generator modelling. The current models in use for UE modelling typically describe this data to 5% accuracy, compared with data uncertainties of less than 1%.

The EPOS MC generator, specialised for simulation of inclusive soft QCD processes, displays particularly discrepant features as the p_T^{lead} scale increases, casting doubt on its suitability for modelling LHC multiple pp interactions despite currently providing the best description of minimum-bias data. Further information about MC generator tunes can be found in [9].

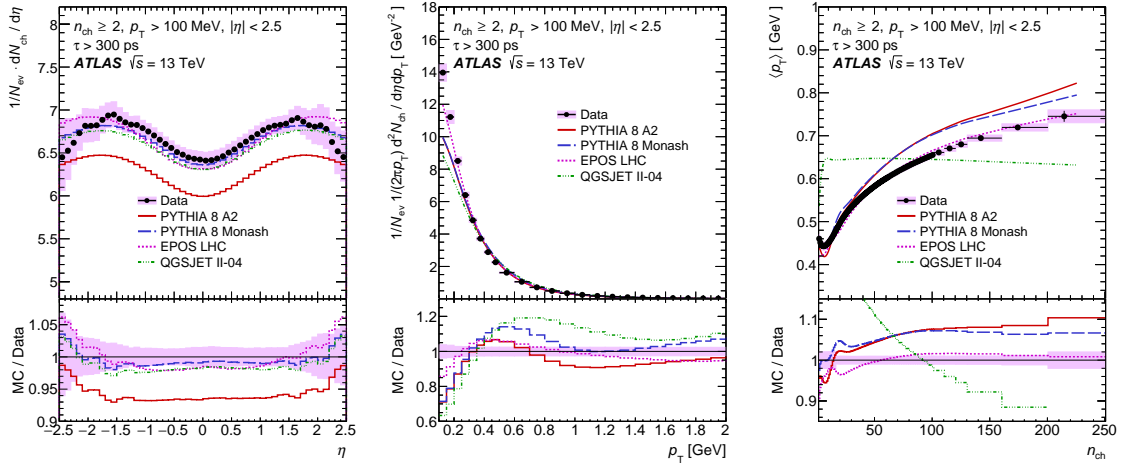


Figure 4: Primary charged-particle multiplicities as a function of (a) pseudorapidity and (b) transverse momentum, (c) the mean transverse momentum p_T versus multiplicity for events with at least two primary charged particles with $p_T > 100$ MeV and $|\eta| < 2.5$, each with a lifetime $\tau > 300$ ps. The vertical bars represent the statistical uncertainties, while the shaded areas show statistical and systematic uncertainties added in quadrature [7].

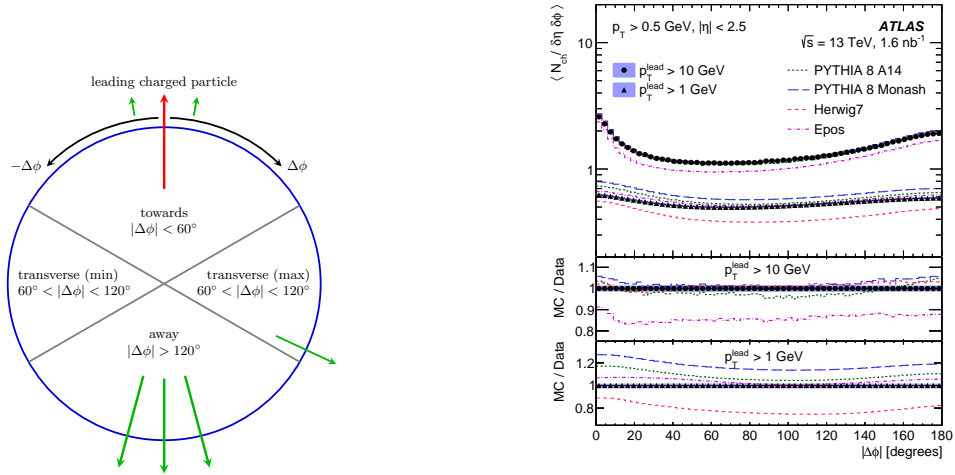


Figure 5: Left: Definition of regions in the azimuthal angle with respect to the leading (highest- p_T) charged particle, with arrows representing particles associated with the hard scattering process and the leading charged particle highlighted in red. Right: Distribution of mean charged-particle density as a function of $|\Delta\phi|$ (with respect to the leading charged particle) for $p_T^{\text{lead}} > 1\text{ GeV}$ and $p_T^{\text{lead}} > 10\text{ GeV}$ separately, with comparisons to MC generator models [8].

4 Identified particle spectra

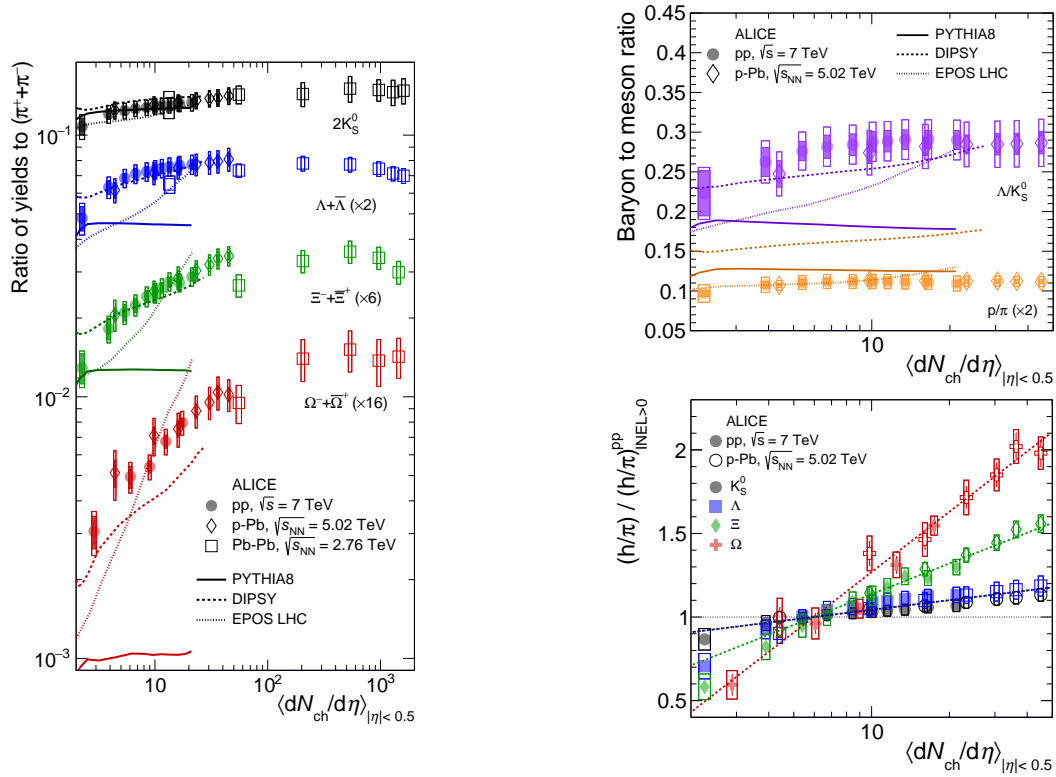


Figure 6: Left: p_T -integrated relative yields w.r.t. the pion ($\pi^+ + \pi^-$) production as a function of charged-particle density measured in $|\eta| < 0.5$. The error bars show the statistical uncertainty, whereas the empty and dark-shaded boxes show the total systematic uncertainty and the contribution uncorrelated across multiplicity bins, respectively. Top right: Ratio of baryon to meson yield compared with MC predictions. Bottom right: Phenomenological fit of the charge multiplicity dependence of the relative yield w.r.t. the pion production [10].

ALICE Collaboration presented the first observation of strangeness enhancement in high-multiplicity pp collisions [10]. The measurement shows that the integrated yields of strange and multi-strange particles relative to pions increases significantly with the event charged-particle multiplicity (Figure 6, left), and that they are in remarkable agreement with p-Pb collision results indicating that the phenomenon is related to the final system created in the collision. In high-multiplicity events strangeness production reaches values similar to those observed in Pb-Pb collisions. The multiplicity dependence is best described by the DIPSY model which however overestimates the yield of protons w.r.t. the pion production (Figure 6, top right).

5 Particle correlations

The particle yields corresponding to the near-side long-range correlations are measured by the CMS Collaboration [11] in pp collisions at $\sqrt{s} = 13$ TeV and compared with previous measurement at $\sqrt{s} = 7$ TeV and with the pPb and PbPb data (Figure 7). The observed yields have approximately linear dependence on the event charge multiplicity for multiplicity above ~ 40 . Further measurements of the near-side correlations can be found in [12], [13], [14]. A study of long-range correlations with the subevent cumulant method finds a close similarity between the multiplicity dependence of the number of sources in pp and pPb collisions [15].

Charge-dependent azimuthal correlations of the same- and opposite-sign particle pairs with respect to the

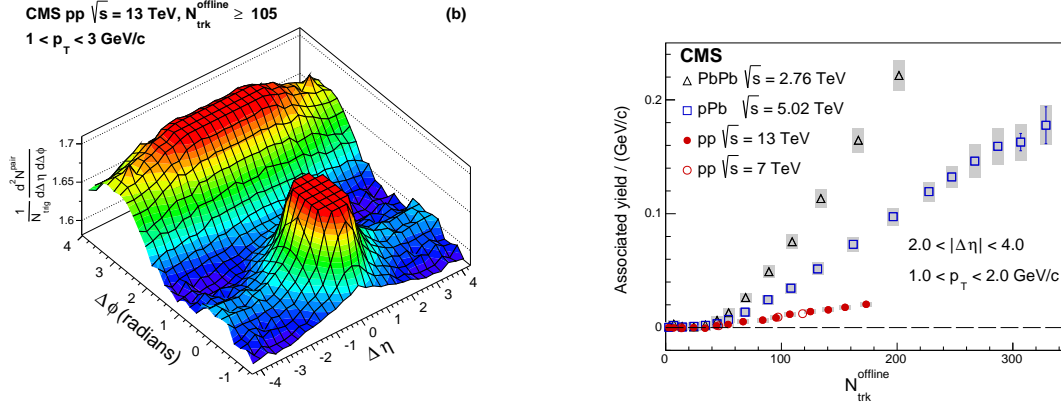


Figure 7: Left: The 2-dim $(\Delta\eta, \Delta\Phi)$ two-particle correlation functions for pairs of charged particles both in the range $1 < p_T < 3$ GeV/c, for charged multiplicity above 105. The sharp peaks from jet correlations around $(\Delta\eta, \Delta\Phi) = (0,0)$ are truncated to better illustrate the long-range correlations. Right: Associated yields of long-range near-side two-particle correlations, averaged over $2 < |\Delta\eta| < 4$. The error bars correspond to the statistical uncertainties, while the shaded areas denote the systematic uncertainties. Note that there are PbPb points above the upper vertical scale, which are not shown for clarity [11].

second-order event plane have been measured in pPb and PbPb collisions at $\sqrt{s_{NN}} = 5.02$ TeV by the CMS experiment at the LHC [16]. Correlations are extracted via a three particle correlator as functions of the $\Delta\eta$ and the charged-particle multiplicity of the event. The differences between the same- and the opposite-sign particle pairs agree for pPb and PbPb collisions (Figure 8), possibly indicating a common underlying mechanism that generates the observed correlation. These results challenge the CME interpretation for the observed charge-dependent azimuthal correlations in nucleus-nucleus collisions at RHIC and the LHC.

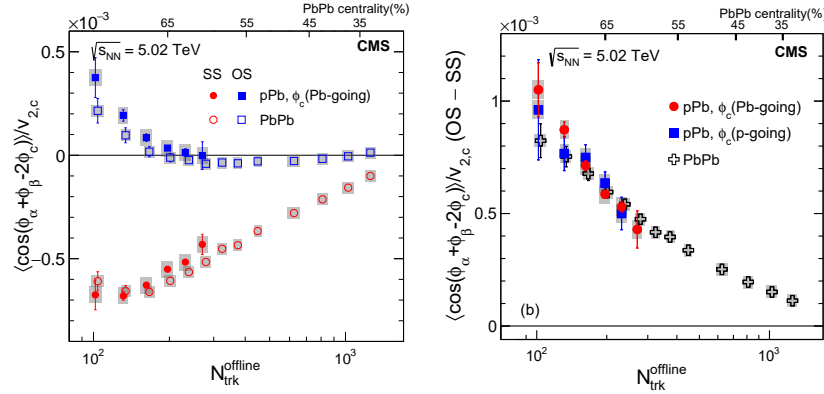


Figure 8: Left: the same-sign (SS) and opposite-sign (OS) three-particle correlators averaged over $|\eta_\alpha \eta_\beta| < 1.6$. Right: their difference as a function of charged multiplicity in pPb and PbPb collisions [16].

Another example of a measurement challenging the conventional interpretation is the study of ordered hadron chains [17]. The measurement isolates the source of two-particle correlations at low four-momentum difference with help of charge-ordered hadron triplets with minimized mass (Figure 9). The correlations are shown to be compatible with the signature of helical QCD string fragmenting into a set of ground-state pions. The measurement offers an alternative explanation of the enhanced production of close like-sign pairs, traditionally attributed to the Bose-Einstein effect [18].

Two-particle angular correlations of identified particles were measured in proton-proton collisions at $\sqrt{s} = 7$

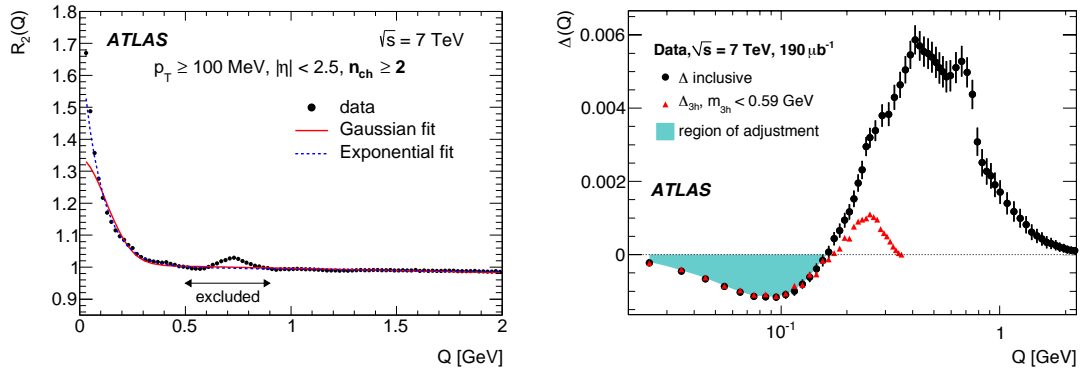


Figure 9: The enhanced production of same-sign particle pairs analysed (left) as a signature of the Bose-Einstein interference [18], via the ratio of same-sign and opposite-sign pair distributions, and (right) as a secondary effect of correlations between adjacent hadrons in the study of ordered hadron chains [17], via the subtraction of same-sign pair distribution from the opposite-sign pair distribution.

TeV by ALICE Collaboration [19]. The analysis was carried out for pions, kaons, protons, and lambdas, for all particle/anti-particle combinations in the pair. Data for mesons exhibit an expected peak dominated by effects associated with mini-jets and are well reproduced by general purpose Monte Carlo generators. However, for baryon-baryon and anti-baryon-anti-baryon pairs, where both particles have the same baryon number, a near-side anti-correlation structure is observed instead of a peak (Figure 10). This effect is interpreted in the context of baryon production mechanisms in the fragmentation process. It currently presents a challenge to Monte Carlo models and its origin remains an open question.

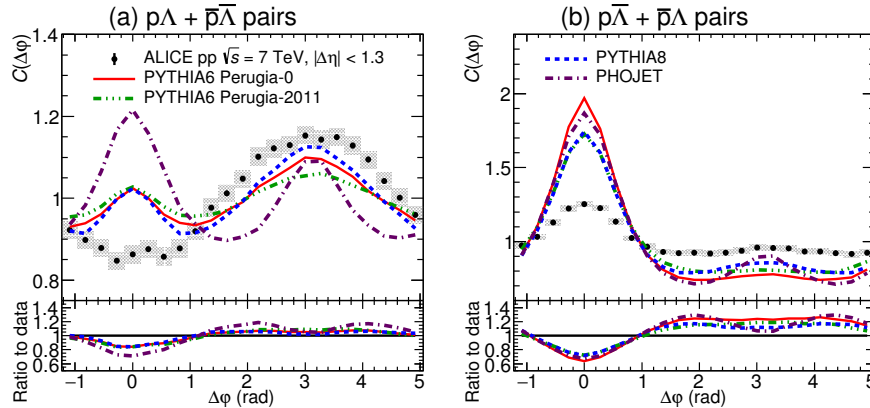


Figure 10: Example of anti-correlations observed for baryon pairs. $\Delta\eta$ integrated projection of correlation functions for combined pairs of (left) $p\Lambda + \bar{p}\bar{\Lambda}$ and (right) $p\bar{\Lambda} + \bar{p}\Lambda$ obtained from ALICE pp collision data and four Monte Carlo models (PYTHIA6 Perugia-0, PYTHIA6 Perugia-2011, PYTHIA8 Monash, PHOJET) at $\sqrt{s} = 7$ TeV [19].

6 Conclusions

A large variety of ongoing measurements bring new insights and constraints to our understanding of the hadron production. There are still quite a few unresolved problems, but we possess a wealth of data which will gradually help us to shed light on rules governing the hadronization, which may explain many similarities

observed between pp, pPb and PbPb collisions, and the soft interactions in general.

Many thanks to all contributing authors !

References

- [1] G. Aad *et al.* [ATLAS Collaboration], Phys. Lett. B 761 (2016) 158, [arXiv:1607.06605].
- [2] G. Antchev *et al.* [TOTEM Collaboration], Phys. Rev. Lett. 111 (2013) 012001.
- [3] G. Antchev *et al.* [TOTEM Collaboration], Eur. Phys. J. C 76 (2016) 661, [arXiv:1610.00603].
- [4] G. Aad *et al.* [ATLAS Collaboration], Phys. Rev. Lett. 117 (2016) 182002, [arXiv:1606.02625].
- [5] V. Khachatryan *et al.* [CMS Collaboration], Phys. Lett. B 759 (2016) 641, [arXiv:1509.03893].
- [6] V. Khachatryan *et al.* [CMS Collaboration], JHEP 08 (2017) 046, [arXiv:1701.08695].
- [7] G. Aad *et al.* [ATLAS Collaboration], Eur. Phys. J. C 76 (2016) 502, [arXiv:1602.01633].
- [8] G. Aad *et al.* [ATLAS Collaboration], JHEP 03 (2017) 157, [arXiv:1701.05390].
- [9] V. Khachatryan *et al.* [CMS Collaboration], Eur. Phys. J. C 76 (2016) 155, [arXiv:1512.00815].
- [10] J. Adam *et al.* [ALICE Collaboration], Nature Physics 13 (2017) 535-539, [arXiv:1606.07424].
- [11] V. Khachatryan *et al.* [CMS Collaboration], Phys. Rev. Lett. 116 (2016) 172302, [arXiv:1510.03068].
- [12] J. Adam *et al.* [ALICE Collaboration], Phys. Rev. C 96 (2017) 034904, [arXiv:1609.06667].
- [13] G. Aad *et al.* [ATLAS Collaboration], Phys. Rev. Lett. 116 (2016) 172301, [arXiv:1509.04776].
- [14] R. Aaij *et al.* [LHCb Collaboration], Phys. Lett. B 762 (2016) 473-483, [arXiv:1512.00439].
- [15] M. Aaboud *et al.* [ATLAS Collaboration], CERN-EP-2017-160, [arXiv:1708.03559].
- [16] V. Khachatryan *et al.* [CMS Collaboration], Phys. Rev. Lett. 118 (2017) 122301, [arXiv:1610.00263].
- [17] G. Aad *et al.* [ATLAS Collaboration], [arXiv:1709.07384], submitted to Phys. Rev. D.
- [18] G. Aad *et al.* [ATLAS Collaboration], Eur. Phys. J. C 75 (2015) 466, [arXiv:1502.07947].
- [19] J. Adam *et al.* [ALICE Collaboration], Eur. Phys. J. C 77 (2017) 569, [arXiv:1612.08975].